Journal of The Electrochemical Society, **152** (3) A570-A576 (2005)
0013-4651/2005/152(3)/A570/7/$7.00 © The Electrochemical Society, Inc.

A Kinetic Study of the Oxygen Reduction Reaction at $LaSrMnO_3$-YSZ Composite Electrodes

Anne C. Co,* Shen Jiang Xia, and Viola I. Birss**,z**

Department of Chemistry, The University of Calgary, Calgary, Alberta T2N 1N4, Canada

The primary focus of this paper is on the establishment of reliable methods for the determination of the mechanism and kinetics of the oxygen reduction reaction (ORR) at solid oxide fuel cell cathodes consisting of lanthanum strontium manganite [$(La_{0.8}Sr_{0.2})_{0.98}MnO_3$, LSM] in a 50 vol % mixture with yttria-stabilized zirconia electrolyte (LSM-YSZ composite). Techniques used include half-cell cyclic voltammetry and electrochemical impedance spectroscopy (EIS) methods in a variable p_{O_2} atmosphere at temperatures ranging from 600 to 900°C. The exchange current densities for the ORR, determined both from the low and high field cyclic voltammetry data and from the charge-transfer resistance from EIS data, are shown to agree closely, yielding an apparent activation energy of *ca.* 120 kJ/mol for the ORR at these composite cathodes. No evidence for diffusion-controlled reactions is seen under the conditions of our work. In this paper we also show the theoretically predicted impact of temperature on the Tafel slope, as well as on the potential range over which the low- and high-field approximations, are valid.
 [DOI: 10.1149/1.1859612]

Manuscript submitted July 13, 2004; revised manuscript received August 24, 2004. Available electronically January 26, 2005.

The typical anode and cathode materials employed in solid oxide fuel cells (SOFCs) consist of Ni mixed with Y_2O_3-stabilized ZrO_2 electrolyte (Ni-YSZ) and lanthanum strontium manganite ($LaSrMnO_3$, LSM) mixed with YSZ in a 50 vol % mixture, respectively. This results in highly porous composite electrodes with an extensive triple phase boundary (TPB),[1-4] where the gas, the electrode, and the YSZ electrolyte meet.

Over the last few decades, the kinetics and mechanism of the oxygen reduction reaction (ORR) at LSM-YSZ cathodes have been investigated primarily with the use of electrochemical impedance spectroscopy (EIS), and less commonly using dc polarization techniques. While there are discrepancies in the literature regarding the interpretation of these electrochemical data, it is generally accepted that the ORR occurs at the TPB.[2-5] However, other groups[5,6] have suggested that the ORR can occur anywhere on the LSM surface due to its low but finite oxygen ion conductivity.

It is often assumed that the mechanism of the ORR first involves the adsorption of O_2 on the LSM surface.[7,8] This is followed by the dissociation of O_2 to two O atoms, followed by a series of electron-transfer steps, reducing O to O^{2-}, which is transported across the electrolyte. It has also been reported[9] that the ORR occurs in two steps, and that O^- surface diffusion is the dominant process at low overpotentials, while in other work[10-12] a charge-transfer step was proposed as rate determining. Others[13-15] have suggested that a dissociative adsorption step may be rate determining at LSM cathodes.

Activation energies (E_a) for the ORR on LSM deposited on YSZ (LSM/YSZ) or for LSM-YSZ composites have been reported to be between 100 and 200 kJ/mol;[16,17] this range in values may be related to different electrode preparation methods or different cathode compositions employed by various research groups. ORR Tafel slopes, rarely reported in the SOFC literature, are seen to be 250-450 mV/dec of current at both dense and porous LSM (noncomposite) cathodes (deposited on YSZ) at temperatures of 700-950°C.[18-20] In fact, the expected Tafel slope, as well as the potential range over which exponential i/E behavior should be observed, are strongly temperature dependent, as will be shown. Indeed, the Tafel slope can be a useful tool for interpreting reaction mechanisms of electrochemical reactions.

The present research has focused primarily on efforts to obtain reliable kinetic data using both EIS and cyclic voltammetric (CV) data [both low-field (linear approximation of Butler-Volmer equation) and high-field (back reaction can be neglected) approaches] for the ORR at LSM-YSZ composite cathodes. It is shown that all three methods yield valid kinetic data and similar activation energies for the ORR for cathodes prepared in-house and at Fuel Cell Energy, Ltd., (FCE, formerly Global Thermoelectric, Inc.) to specified requirements using commercial processing equipment. No evidence for diffusion-controlled reactions is seen under the conditions of our work. In this paper, we also consider the theoretically predicted impact of temperature on the Tafel slope, as well as on the potential ranges over which the low- and high-field approximations are valid, with low error.

Experimental

The LSM-YSZ composite working electrodes (WEs) used in our studies were either donated by FCE for the purposes of this project, or prepared in-house. FCE electrodes were prepared by mixing equal volumes of $(La_{0.8}Sr_{0.2})_{0.98}MnO_3$ (Praxair Ceramics, Inc.) with 8 mol % Y_2O_3 doped ZrO_2 (8YSZ, Tosoh) in alcohol and ballmilling. The slurry was screen printed (200 mesh stainless steel) symmetrically on each side of a 50 × 50 mm, 0.2 mm thick YSZ plate (Fig. 1), covering 40 × 40 mm (1600 mm^2); this was done twice, resulting in two layers of the composite material. A pure LSM layer (*ca.* 15 μm thick) was screen printed on top of the LSM-YSZ composite layer to serve as a conducting current collector (Fig. 1). The cathode half-cell was then sintered in air at 1150°C for 2 h. These electrodes (sometimes prior to sintering) were cut into smaller pieces, providing a working area between 3 and 20 mm^2.

In-house electrodes were prepared by screen printing (1100 silk mesh) a LSM-YSZ slurry (50 wt % LSM) on each side of a 0.2 mm thick presintered commercial YSZ (Tosoh) plate, or on presintered in-house pressed, 12 mm diam, 0.6 mm thick YSZ pellets, covering between 5 and 50 mm^2. In-house electrodes were sintered at 1100°C for 2 h before another thin layer of LSM was screen printed on top of the composite layer to serve as the current collector. This procedure was followed again by sintering at 1100°C for 2 h.

The two sides later served as the WE and counter electrodes (CE). Pt paste (Ferro 4082) was also applied to the YSZ on the same side as the WE to serve as a reference electrode (RE). The RE was normally placed 2-5 mm from the WE (Fig. 1), ensuring that this distance was at least three times the thickness of the electrolyte.[21] Pt gauze, attached to a Pt wire, was then press-contacted to the LSM/LSM-YSZ and Pt paste electrodes with the aid of a spring-loaded ceramic cap, thus serving as the final current collector.

Half-cell experiments, involving air or oxygen with p_{O_2} ranging from 0.002 to 1 atm, were carried out over temperatures ranging from 450 to 1000°C in a tube furnace (Lindberg). Cyclic voltammetry (CV) measurements (1-100 mV/s) were performed using an EG&G PARC 273 potentiostat or a Solartron 1287 interface, with control and data collection handled by Corrware software (version

* Electrochemical Society Student Member.
** Electrochemical Society Active Member.
z E-mail: birss@ucalgary.ca

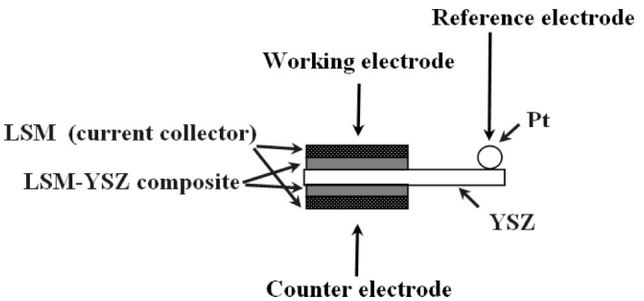

Figure 1. Schematic of three-electrode setup for FCE or in-house LSM/LSM-YSZ/YSZ/LSM-YSZ/LSM cell.

2.7a). The IR drop originating from the electrolyte resistance was compensated for by a postfactum correction of the CVs, using the series resistance obtained from the EIS data, in order to establish the resistance-free i/E characteristics. For the EIS analysis, a Solartron 1255 frequency response analyzer was coupled with the potentiostat. The frequency range employed was 0.1 Hz to 500 kHz, and the measurements were made between 0 and −0.4 V dc bias *vs.* the open-circuit potential (OCP) or *vs.* the Pt RE, using a perturbation amplitude of 10 mV root-mean-square (rms). The EIS measurements and fitting analysis were controlled with commercial software (ZPLOT version 2.7).

The thickness and porosity of the LSM-YSZ composites were determined using a Philips/FEI environmental scanning electron microscope (Health Sciences Center, University of Calgary). An accelerating voltage of 20 kV and a high vacuum of 2×10^{-4} Torr were generally employed. The FCE-supplied composite cathodes were mechanically fractured before mounting them on Al stubs using conducting carbon tape (E. T. Enterprises). A thin layer of Au/Pd, Pt, or C was sometimes sputtered onto the sample to improve surface conductivity. The samples were also tilted in the scanning electron microscopy (SEM) chamber for a better estimation of the film thicknesses.

Theoretical Considerations

Electrochemical methods for determining exchange current (i_o).—The exchange current density, i_o, the intrinsic ORR rate, can be obtained electrochemically[22] using ac impedance spectroscopy (EIS), as well as by using the low-field and high-field approximations to the Butler-Volmer equation

$$i = i_o[e^{\alpha_a F\eta/RT} - e^{-\alpha_c F\eta/RT}] \quad [1]$$

where[23,24]

$$\alpha_a + \alpha_c = \frac{n}{\upsilon} \quad [2]$$

and for the reduction of oxygen

$$\alpha_c = \frac{\gamma}{\upsilon} + r\beta \quad [3]$$

and i_o can also be represented by Eq. 4[23]

$$i_o = \frac{I_o}{A} = \text{const} \quad nFC\frac{kT}{h}e^{-(\Delta G^{o,c\neq} + \beta F\varphi_{equil}/RT)} = Be^{-(Ea/RT)} \quad [4]$$

Here i is the measured ORR current density per electrode geometric area, A, α_a and α_c are the anodic and cathodic transfer coefficients, respectively, η is the overpotential, n is the total number of electrons passed in the reaction, γ is the number of electrons transferred before the rate-determining step (rds) in the reaction sequence, υ reflects the number of times the rds occurs for one occurrence of the full reaction, r is the number of electrons transferred during the rds, β is the symmetry coefficient of the rds (normally assumed to be 0.5), C is the concentration of the reactant, k is the Boltzmann constant, h is the Planck constant, $\Delta G^{o,c\neq}$ is the chemical energy of activation, ϕ_{equil} is the equilibrium potential difference across the LSM/YSZ interface, B is the combined pre-exponential term, and F, R, and T have their usual meaning. Based on these considerations, the Tafel slope increases with temperature (Eq. 1). However, the effect of the temperature dependence of the Tafel slope on the rate of the ORR is outweighed by the substantial effect of temperature on i_o (Eq. 4). This results in an overall significant increase in the ORR rate with increasing temperature.

From experimental i/E data, i_o can be obtained at both small and large overpotentials. In the low-field case, with ≤2% error, the Butler-Volmer (Eq. 1) can be linearized when

$$\eta \leqslant \frac{0.2(RT)}{\alpha F} \quad [5]$$

leading to the low-field equation

$$i = i_o\frac{Fn}{RT\upsilon}\eta \quad [6]$$

In the case of a simple one-electron reaction, $\beta = 0.5$, $\gamma = 0$, $\nu = 1$, and thus $\alpha = 0.5$. The linear low-field region (Eq. 5) then extends to ±10 mV at 25°C, ±27 mV at 500°C, and ±37 mV at 800°C. Notably, for higher α values, the linear range of potential is narrowed at all temperatures.

i_o can also be deduced from the charge-transfer resistance (R_{ct}) obtained from impedance data, using Eq. 7. As impedance measurements are obtained by perturbing the system typically within only ±10 mV rms *vs.* the OCP, Eq. 7 is derived from the low-field approximation of Eq. 6

$$i_o = \frac{1}{R_{ct}}\frac{RT\upsilon}{Fn} \quad [7]$$

At higher overpotentials, the back reaction (O_2 evolution) can be ignored, leading to Eq. 8, from which i_o can also be readily obtained

$$i = i_o e^{-\alpha_c F/RT\eta} \quad [8]$$

$$\eta \geqslant \ln(99)\frac{RT\upsilon}{Fn} \quad [9]$$

The overpotential above which the high-field approximation is valid is also temperature dependent, as seen in Eq. 9. For example, allowing <1% error, a minimum overpotential of 427 mV (assuming n/ν of 1) is necessary to reach the Tafel region at 800°C, compared to 118 mV at 25°C. Notably, the ratio of n/ν, indicative of an assumed reaction mechanism, also influences the onset potential of the Tafel region. For example, for n/ν values of 4/1, 4/2, and 4/3, the minimum overpotential is 107, 213, and 320 mV, respectively, at 800°C. These calculations demonstrate that a large overpotential must be reached before the high-field approximation of the Butler-Volmer equation can validly be used to give i_o at the high temperatures typical of SOFC conditions

Results and Discussion

Morphology of LSM-YSZ composite electrodes.—An SEM image of the cross section of the FCE composite LSM-YSZ electrode is shown in Fig. 2. The total thickness of the composite electrode layer is *ca.* 15 μm, with particle diameters ranging between 0.5 and 0.9 μm, while the current collector layer (pure LSM) is *ca.* 10 μm thick. In the case of the in-house LSM-YSZ (SEM image not shown), the total thickness of the composite layer was *ca.* 30 μm, with particle diameters of *ca.* 0.2 μm and a current collector layer thickness of *ca.* 30 μm. The distribution of YSZ and LSM particles in both the

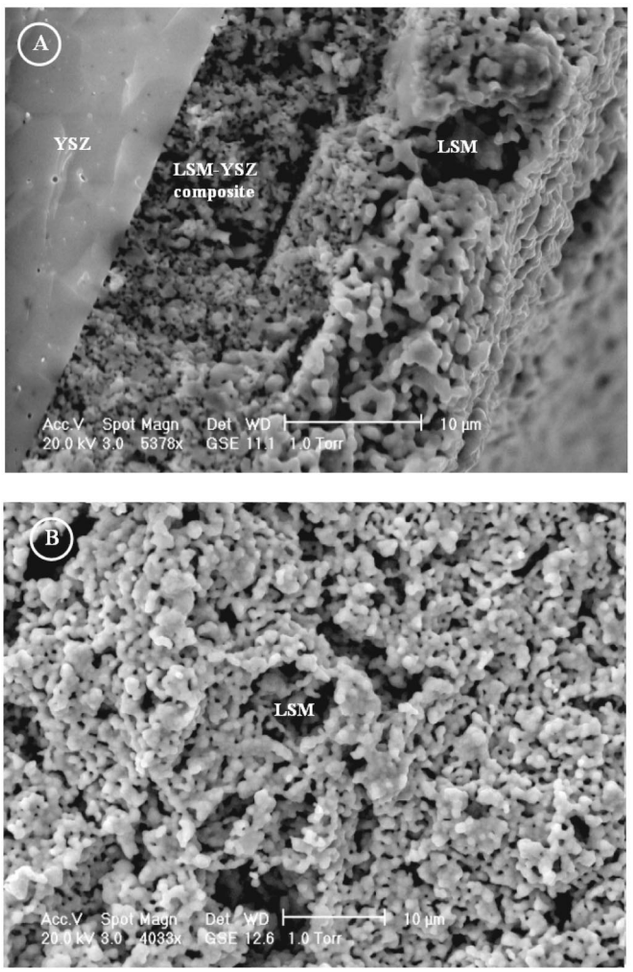

Figure 2. (a) FCE LSM-YSZ composite cathode cross section. Shown from left to right is the dense YSZ layer, two layers of porous LSM-YSZ composite, and an outer layer of LSM. (b) Top view of the highly porous LSM current collector.

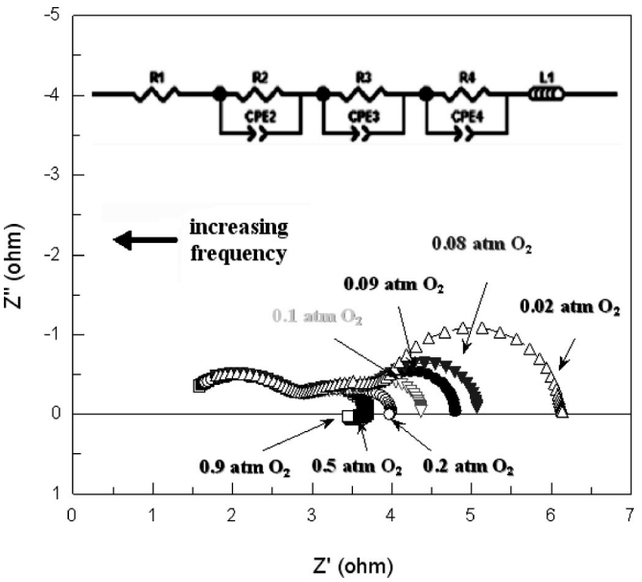

Figure 3. Complex impedance spectra of FCE LSM-YSZ composite cathode (*ca.* 5 mm^2 apparent WE area) on YSZ disk at 800°C at OCP (10 mV rms), at various O_2 partial pressures: (■) 0.9, (□) 0.5, (○) 0.2, (▽) 0.1, (●) 0.09, (▼) 0.08, and (△) 0.02 atm.

FCE and in-house composite electrode is quite uniform, as was seen from the similar relative ratios of La to Zr obtained from EDX analyses carried out at a range of locations. The porosity of the composite electrode is lower than that of the outer current-collecting LSM layer, as desired for good oxygen access to the active layer. After subjecting the FCE and in-house LSM-YSZ composite to electrochemical measurements at high temperatures, no other interfacial layer or products, *e.g.*, $La_2Zr_2O_7$, which would be resistive to electron transfer,[25,26] were seen to have formed.

Determination of ORR kinetics from the exchange currents (i_o).—*ORR kinetics from EIS data*.—Figure 3 shows a family of complex impedance plots obtained for the ORR at a FCE LSM/LSM-YSZ composite electrode at the OCP, 800°C, and at various oxygen partial pressures. Above $p_{O_2} = 0.5$ atm, only two semicircles are seen, while at lower oxygen partial pressures, a third semicircle is seen at low frequencies. The size of the low-frequency semicircle increases (higher resistance) with decreasing O_2 partial pressure, indicating that it is related directly to the ORR.

An inductive response, commonly attributed in the literature to a dynamic increase in surface area or activity, such as in pitting corrosion,[27] the nucleation of active sites,[28] or the formation of electronic defects,[7] appears at low frequencies when the O_2 partial pressure is greater than 0.5 atm. In the SOFC literature, the low-frequency inductor has been attributed to the activation of a passive layer at the electrode surface,[29] or specifically for the $La_{0.5}Sr_{0.5}MnO_3$ system,[30] to the adsorption of several species at the same site. In our data, while the low-frequency inductor is not always observed, it is often correlated with the appearance of a hysteresis loop (counter-clockwise response) in the CV measurements, indicating a possible increase in the active area during polarization.

The EIS data were fitted to the equivalent circuit shown in Fig. 3, with three R/CPE units in series with a fourth resistor (R_1) and an inductor.[22] A constant phase element (CPE) represents a nonideal capacitor, *e.g.*, of the double layer at a nonplanar TPB, and the associated *n* parameter indicates the CPE's similarity to a true capacitor, for which *n* is 1. The CPE values are obtained by fitting experimental data to Eq. 10

$$Z = \frac{1}{\mathrm{CPE}(j\omega)^n} \qquad [10]$$

Incorporated in R_1 is the uncompensated resistance between the RE and the WE, the contact resistance between the Pt leads to the WE current collector, and the resistance of the leads. The inductor reflects the low-frequency behavior seen at high oxygen partial pressures in Fig. 3 also usually seen at Pt/YSZ interfaces in O_2.[31]

R_2 and R_3, originating from the high and mid frequency arcs and independent of the O_2 partial pressure, are associated with the Pt/LSM and LSM/LSM-YSZ interfaces,[22,32] or with grain boundaries within the ceramic materials.[33] R_4, which arises from the low frequency arc and showing a strong dependence on the oxygen partial pressure (Fig. 3), is assigned to the charge-transfer resistance, R_{ct}, which is related directly to the ORR i_o (Eq. 7). The i_o values obtained through this means are given in Table I.

Similar to the FCE cathode (Fig. 3), a series of semicircles is also observed for the ORR at the in-house LSM/LSM-YSZ/YSZ (Fig. 4), but with a smaller R_2/CPE_2 semicircle size and a less well-defined R_3/CPE_3 feature. This may arise from the different thicknesses of the LSM and LSM-YSZ layers or the different number of layers for these two types of electrodes. Again, only the low-frequency R_4/CPE_4 elements change with the O_2 partial pressure, giving the i_o value, consistent with the approach of Jørgensen and Mogensen.[16] Due to the relatively small value obtained for the medium-

Table I. i_o and i values measured at −30 mV for the ORR at in-house LSM/LSM-YSZ electrodes using low-field CV, high-field CV, and EIS measurements at 600-900°C, assuming $n/\nu = 1$.

	i_o (A/cm^2)			
T (°C)	Low-field	High-field	EIS	i at −30 mV
600	4.20×10^{-3}	6.10×10^{-3}	2.40×10^{-3}	-1.1×10^{-3}
700	3.80×10^{-2}	4.30×10^{-2}	3.10×10^{-2}	-8.2×10^{-3}
800	1.60×10^{-1}	1.40×10^{-1}	2.30×10^{-1}	-3.1×10^{-2}
900	4.40×10^{-1}	4.50×10^{-1}	4.30×10^{-1}	-5.9×10^{-2}

frequency-range R_3/CPE_3 unit using a three-arc model, a two-arc model was sometimes used to fit the impedance data obtained for the ORR at the in-house LSM-YSZ/LSM electrode. However, the values for R_1 and R_4/CPE_4 were essentially independent of the choice of equivalent circuit used.

The literature shows that the impedance response for the ORR at LSM-YSZ composites depends strongly on the electrode composition, morphology, and processing parameters.[2,4,9,13,16,19] In general, the high-frequency arc does not display any oxygen dependence, consistent with our work, and has been interpreted as being due to oxygen ion transfer from the electrode to the oxygen ion vacancies of the electrode[14] or to grain boundary resistance of the YSZ component.[33] The assignment of the mid-frequency arc is often inconclusive, although it has sometimes been interpreted as reflecting either oxygen adsorption or dissociation processes.[9,14,33]

Table II shows the values of the key circuit elements as a function of the cell operating temperature for in-house LSM-YSZ composite cathodes. In all cases, it is seen that R_1, R_2, and R_4 decrease dramatically with increasing temperature, as expected. The low-frequency R_4, assigned to the ORR charge-transfer resistance, is converted to i_o using Eq. 7. Most research groups have reported a p_{O_2} dependence of the low-frequency arc, although the interpretation of this arc varies greatly. Juhl *et al.*[34] have attributed the low-frequency arc to a chemical step in the overall ORR, while others have suggested that it reflects the diffusion of O^{2-} to the electrode/electrolyte interface, based on the observed dependence on p_{O_2}.

While both diffusion and activation-controlled steps would be expected to exhibit a linear dependence on the reactant concentration, our low-frequency semicircle is symmetrical and fits properly

Table II. R_1, R_2/CPE_2, and $R_4/CPE_4/n_4$ values for ORR as a function of temperature at in-house LSM-YSZ/LSM cathodes in air.

T (°C)	R_1 (Ω cm^2)	R_2 (Ω cm^2)	CPE_2 (mFs)$^{1-n}$/cm^2	R_4 (Ω cm^2)	CPE_4 (mFs)$^{1-n}$/cm^2	n_4
600	0.8	3.4	9	30	38	0.7
700	0.3	1.3		2		
800	0.13	0.2	7.5	0.4	40	0.7
900	0.08	0.1	2	0.2	12	0.9

to a CPE (with an n value of 0.7-0.9), for both the in-house and FCE cathodes, indicating that the ORR is not diffusion controlled in the present work. Gas flow rates had no effect on either our impedance or CV data, as shown in Fig. 5, again indicating the absence of mass-transfer limitations which would influence the i_o and Tafel interpretation in this work. Also noteworthy are the barely changing CPE_4 values (with $n > 0.7$) at temperatures of 600-800°C (Table II), above which a possible change in the interface may have occurred. Because R_4 is assigned to the R_{ct} of the ORR, CPE_4 can be related to the "double layer" or interfacial area between the cathode and the electrolyte.

ORR kinetics from EIS data.—Figure 6 illustrates the IR-compensated i/η relationship of the ORR at an in-house LSM-YSZ/LSM electrode over a wide range of overpotentials for temperatures from 600 to 900°C (a similar result was seen for the FCE cathodes). The CV response is stable, evidenced by multiple scans of the full potential range and the absence of dynamic hysteresis effects, commonly seen with Pt cathodes.[31] The stability of the CV response with time also verifies that extension to relatively high negative potentials of *ca.* 1 V does not cause any unwanted reactions to occur, which would be expected to have a deleterious effect on the ORR activity.

To verify the EIS data discussed previously (Fig. 3-5), showing that there are no transport limitations present in these experiments, the CVs were collected at a range of sweep rates. Figure 7 shows that these data, even at high current densities, are independent of

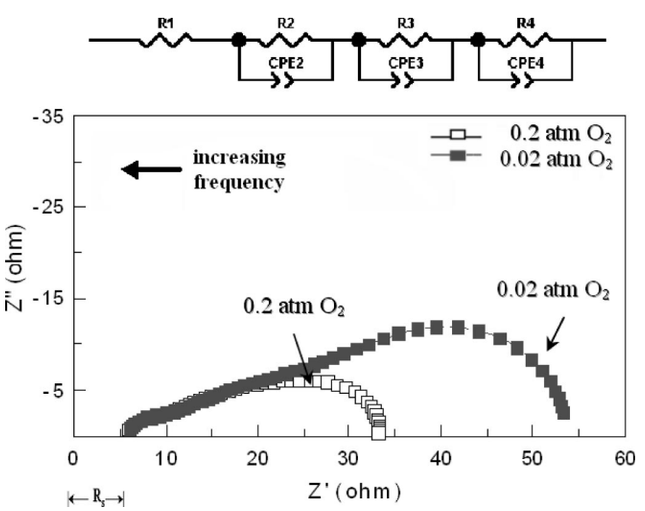

Figure 4. Nyquist plot of ORR at in-house LSM/LSM-YSZ composite/YSZ electrode (*ca.* 6 mm^2 apparent WE area) in air at 800°C in (□) 0.2 p_{O_2} and (■) 0.02 p_{O_2}.

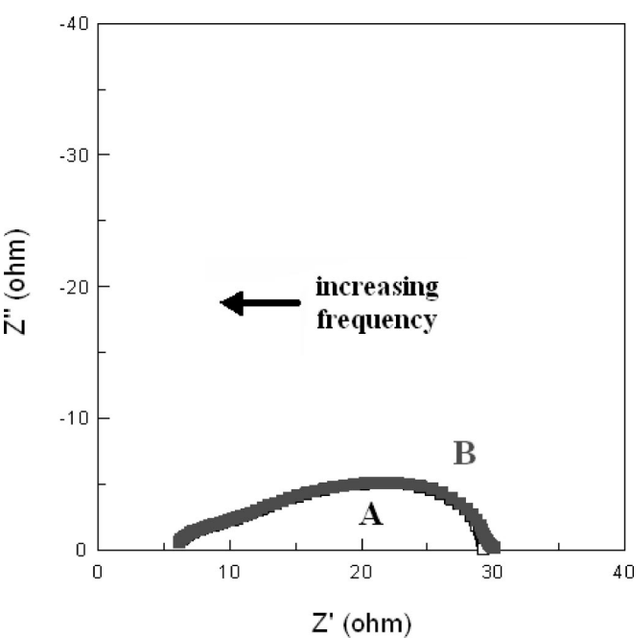

Figure 5. Nyquist plot of ORR at in-house LSM/LSM-YSZ composite/YSZ electrode in air at 800°C in (□) stagnant air and (■) 50 mL/min 0.02 p_{O_2} N2 balance; *ca.* 6 mm^2 apparent WE area.

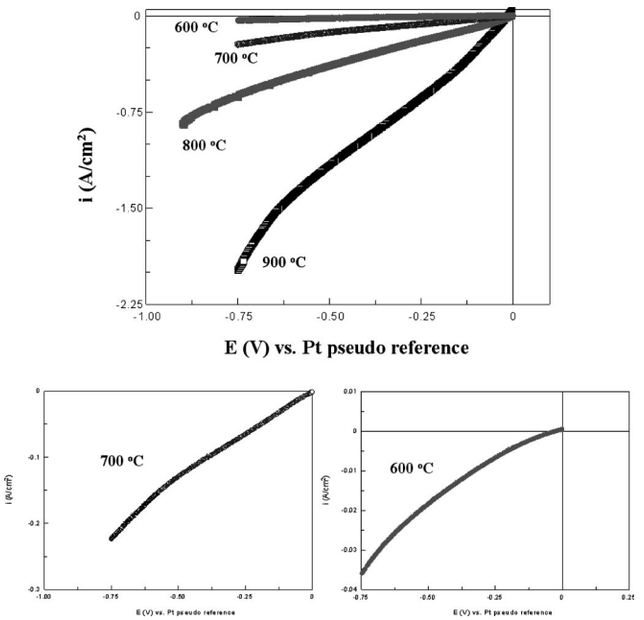

Figure 6. IR-corrected i/E relationship (10 mV/s) of O_2 reduction on in-house LSM/LSM-YSZ composite/YSZ at 600-900°C; 20 mV/s; *ca.* 6 mm^2 apparent WE area. Insets: expanded scales better reveal the Butler-Volmer behavior at 600 and 700°C.

perturbation rate. This indicates that the ORR is indeed activation controlled and that there are no diffusional limitations present under our experimental conditions.

Figure 8 shows the Tafel plot of the four data sets of Fig. 6, demonstrating that a linear Tafel region is indeed obtained and that it appears only at comparatively negative overpotentials, as predicted (Eq. 9). The exponential region should commence at approximately −310 and −430 mV for 500 and 800°C, respectively, assuming $n/\nu = 1$. It can be seen that these predicted onset potentials are closely matched by what is seen experimentally. Figure 8 also shows that the Tafel slopes are high, *e.g.*, 590-830 mV and 940-1000 mV at 600 and 800°C, respectively, significantly larger in value than predicted by the Butler-Volmer equation (250 and 430 mV Tafel

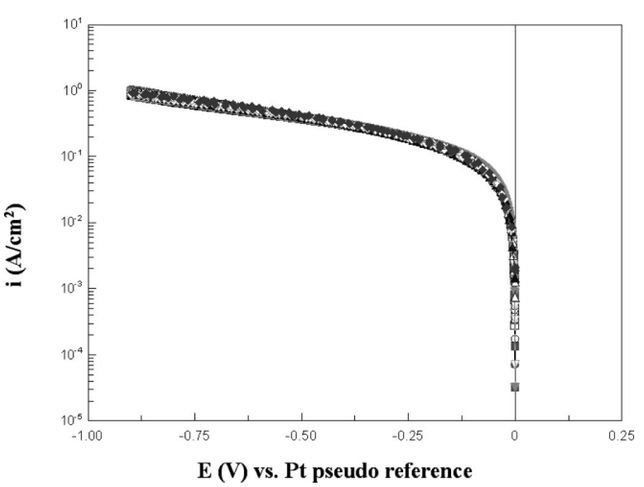

Figure 7. Tafel plots from 1 to 200 mV/s between 0 and −0.9 V (with IR compensation) of the ORR at LSM-YSZ composite electrode (*ca.* 6 mm^2 apparent WE area) on YSZ disk at 800°C in air.

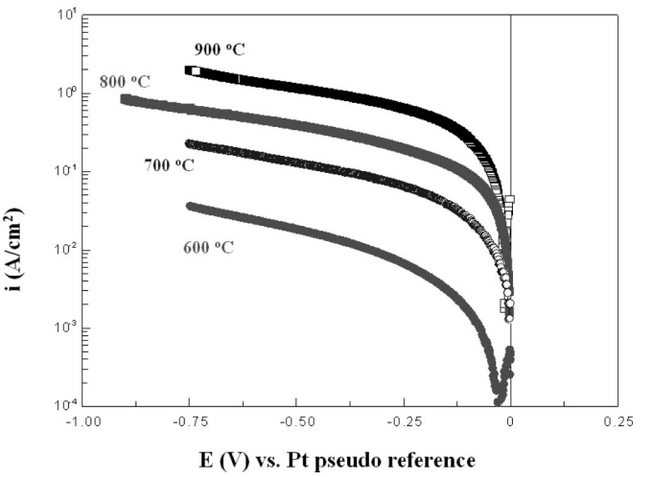

Figure 8. Tafel plot at 10 mV/s for O_2 reduction at in-house LSM/LSM-YSZ composite/YSZ electrode (*ca.* 6 mm^2 apparent WE area) in air at 600-800°C.

slopes for 600 and 800°C, respectively, assuming $\beta = 0.5$). Possible explanations for this anomalous behavior will be presented in another paper, currently in preparation.[35]

The best-fit line through the high-field data points in Fig. 8, using the potential range given in Eq. 9, was extrapolated back to the OCP (0 V *vs.* Pt), yielding i_o, as predicted by Eq. 8. Initially assuming a very simple mechanism for which $n/\nu = 1$, a line was fitted between −430 and −900 mV for the 800°C data in Fig. 8; the minimum overpotentials employed at 600, 700, and 900°C for this analysis were −350, −390, and −470 mV, respectively. Allowing for a wider range of possible mechanisms (n/ν values ranging from 1 to 4), i_o values were again obtained by fitting the best-fit straight line through the high-field data, but now commencing at overpotentials appropriate for the chosen n/η values. Table I shows that the i_o values obtained using this approach agreed closely with each other, once the intercepts were corrected for the n/ν values, thus confirming the validity of this approach.

Under low-field conditions, i_o was obtained by applying Eq. 6 to the low-overpotential data (within ±30, 34, 37, and 40 mV *vs.* OCP at 600, 700, 800, and 900°C, respectively) of Fig. 6, which were compensated for the IR drop between the WE and RE using the R_1 value obtained from impedance measurements. However, to obtain the i_o values, shown in Table I (and assuming n/ν to be 1), these data had to also be further corrected for the impedance-determined R_2 and R_3 values at each temperature.

The i_o values obtained for the ORR at the same in-house LSM/LSM-YSZ electrode using the three methods described above are given in Table I. The results show a good correlation between the three techniques, indicating the validity of these measurements and also demonstrating the stability of these composite cathode materials and their responses. It is also observed that i_o, as well as the absolute current values at −30 mV, increases significantly with temperature, as expected.

Unfortunately, it is impossible to compare the ORR activity of these LSM/LSM-YSZ electrodes with that of Pt/YSZ cathodes.[31] This is because we do not know the active TPB area of either of these electrode materials. In the case of porous Pt paste spread on YSZ, the active interface is only at the perimeters of islands of Pt which are in good contact with the YSZ disk, and which are also accessible to oxygen and in good contact with the Pt mesh current collector. For the LSM/LSM-YSZ materials, the active interface is anticipated to be much larger, considering the composite nature of this coating and the ionic and electronic conductivity of LSM. Even so, it is interesting that the i_o values (based on geometric areas) for

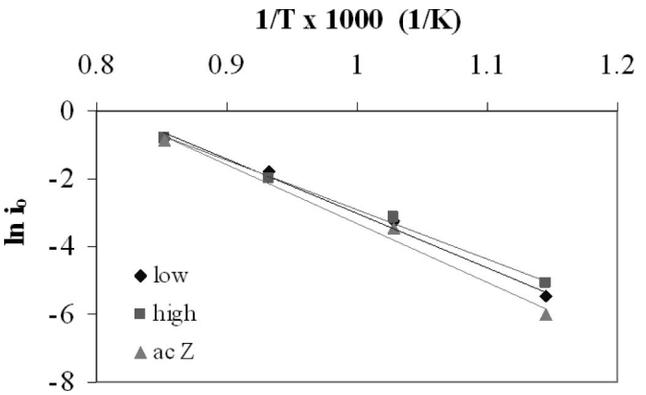

Figure 9. Arrhenius plots for ORR at in-house LSM/LSM-YSZ composite/YSZ electrodes in air. i_o was obtained using the low-field, high-field, and EIS techniques for n/ν of 1.

the ORR are approximately ten times higher at Pt paste on YSZ *vs.* the LSM/LSM-YSZ cathodes (Table I). As the latter composite electrodes are expected to have the much larger TPBs, this indicates the likely superior catalytic activity of Pt *vs.* LSM as an ORR cathode.

Determination of ORR activation energies from i_o values.—Figure 9 shows the Arrhenius plots for the i_o values collected at in-house LSM/LSM-YSZ electrodes between 600 and 900°C, using the three methods discussed previously, and assuming a n/ν ratio of 1. The apparent activation energy of the ORR, obtained from the slope of these plots via the simplifying equation (Eq. 4), is between 120 and 150 kJ/mol (29-36 kcal/mol or 0.3-0.37 eV).[22] Although not shown, the n/ν ratio does not affect the value of the ORR activation energy, regardless of whether the low-field, high-field, or EIS method was employed. Also, the linearity of the plots in Fig. 9 again indicates that the in-house LSM-YSZ composite electrodes are stable as a function of temperature and other experimental conditions.

The ORR activation energy obtained for the in-house LSM-YSZ composite is reasonable and compares well to the E_a values of 100-200 kJ/mol reported in the literature.[13,17] For example, an E_a of 110 kJ/mol was reported for $La_{0.3}Sr_{0.7}MnO_3$, while a value of 180 kJ/mol was obtained for the ORR at both $La_{0.5}Sr_{0.5}MnO_3$ and $La_{0.7}Sr_{0.3}MnO_3$.[18] A reported E_a of 200 kJ/mol[17,19] was attributed to the dissociation of O_2 at low overpotentials, while an E_a of 160 kJ/mol, along with a $p_{O_2}^{-0.14}$ dependence,[33] was attributed to the slow step being oxygen dissociation and adsorption. Ostergard and Mogensen[14] proposed an oxygen adsorption mechanism, following the Freundlich isotherm, and attributed the medium-frequency arc to the dissociation of adsorbed oxygen molecules. Our previous work with Pt paste on YSZ yielded an ORR E_a value of 120 kJ/mol, a value which has been suggested by others to reflect the slow surface diffusion of O_2 on the Pt surface.[36,37] Overall, in our work, it appears that the ORR activation energy is similar at LSM-YSZ and Pt cathode layers on YSZ. Based on our results to date, including the anomalously high Tafel slopes observed (Fig. 6), we cannot conclusively determine the ORR mechanism and/or rds at our LSM-YSZ cathode materials.

Conclusion

EIS and CV data were collected for LSM-YSZ composite cathodes prepared both in-house and supplied by FCE over the temperature range 600-900°C and at various p_{O_2}. It was conclusively shown that no transport limitations are present in the ORR under the conditions of our experiments. This was seen by a lack of dependence of the CV currents on sweep rate and of the EIS data on the p_{O_2} flow rate, as well as by the absence of any diffusional features in the EIS data, *e.g.*, a Warburg component.

The exchange current densities (based on geometric area) for the ORR at in-house LSM-YSZ composite cathodes were determined from the charge-transfer resistance obtained from the EIS experiments, as well as from both low- and high-field CV data. For a simple mechanism involving the transfer of only one electron and with an electron transfer as the rds, it was shown that at 800°C, the low-field CV range should not exceed ±40 mV *vs.* the OCP. Furthermore, the high-field region does not commence until an overpotential of −430 mV has been exceeded. Based on these limits, the i_o values obtained using all three methods showed close agreement at all temperatures, indicating that our experimental and interpretive approach is correct and also demonstrating good cathode stability.

An apparent activation energy in the range of 120-150 kJ/mol was obtained for the ORR, comparable to literature values at LSM on YSZ, and for both LSM-YSZ and Pt-YSZ composite cathodes. The anomalously high Tafel slopes observed precluded any easy conclusions to be drawn at this point regarding the ORR mechanism. However, this will be the topic of future work.

Acknowledgments

This work was supported by The Alberta Energy Research Institute (AERI) through the Coordination of University Research for Synergy and Effectiveness (COURSE) program. The authors also thank Global Thermoelectric, Inc., (now Fuel Cell Energy, Ltd., Calgary, Canada) for materials, as well as Dr. Mark Cassidy, Dr. Peng Huang, and Dr. Eric Tang, and Anthony Wood and Stephanie Staite, all of Fuel Cell Energy, for their assistance with cell design, provision of materials, and useful discussions. We also thank the National Research Council of Canada (NRC) for the donation of the Pt paste used in this project.

The University of Calgary assisted in meeting the publication costs of this article.

List of Symbols

A	area, cm^2
F	Faraday constant, 96485 C/mol
h	Planck constant, $6.6260755 \times 10^{-34}$ J s
I	current, A
I_o	exchange current, A
i	current density, A/cm^2
i_o	exchange current density, A/cm^2
k	Boltzmann constant, 1.380658×10^{-23} J/K
n	total number of electrons
R	gas constant, 8.31451 J/K mol
r	number of electrons transferred during the rds
T	temperature, K
X	pre-exponential constant
Y	combined pre-exponential term

Greek

α_a	anodic transfer coefficient
α_c	cathodic transfer coefficient
β	symmetry coefficient
$\Delta G^{o,c\neq}$	chemical energy of activation
η	overpotential, E
γ	number of electrons transferred before the rds
ν	stoichiometry of the rds
ϕ_{equi}	equilibrium potential across the interface

References

1. J. Mizusaki, T. Saito, and H. Tagawa, *J. Electrochem. Soc.*, **143**, 3065 (1996).
2. S. Carter, A. Selcuk, R. J. Chater, J. Kajda, J. A. Kilner, and B. C. H. Steele, *Solid State Ionics*, **53-6**, 597 (1992).
3. J. Mizusaki, H. Tagawa, K. Tsuneyoshi, and A. Sawata, *J. Electrochem. Soc.*, **138**, 1867 (1991).
4. K. Sasaki, J. P. Wurth, R. Gschwend, M. Godickemeier, and L. J. Gauckler, *J. Electrochem. Soc.*, **143**, 530 (1996).
5. A. Hammouche, E. Siebert, A. Hammou, M. Kleitz, and A. Caneiro, *J. Electrochem. Soc.*, **138**, 1212 (1991).
6. A. Hammouche, E. Siebert, and A. Hammou, *MRS Bull.*, **24**, 367 (1989).
7. E. J. L. Schouler and M. Kleitz, *J. Electrochem. Soc.*, **134**, 1045 (1987).

8. P. Farby and M. Kleitz, *J. Electroanal. Chem. Interfacial Electrochem.*, **57**, 165 (1974).
9. F. H. van Heuveln, H. J. M. Bouwmeester, and F. P. F. van Berkel, *J. Electrochem. Soc.*, **144**, 126 (1997).
10. H. Y. Lee, W. S. Cho, S. M. Oh, H. D. Wiemhofer, and W. Gopel, *J. Electrochem. Soc.*, **142**, 2659 (1995).
11. R. E. W. Casselton, *J. Appl. Electrochem.*, **4**, 25 (1974).
12. A. J. A. Winnubst, A. H. A. Scharenborg, and A. J. Burggraaf, *Solid State Ionics*, **14**, 319 (1984).
13. E. Siebert, A. Hammouche, and M. Kleitz, *Electrochim. Acta*, **40**, 1741 (1995).
14. M. J. L. Ostergard and M. Mogensen, *Electrochim. Acta*, **38**, 2015 (1993).
15. S. Z. Wang, Y. Jiang, Y. H. Zhang, J. W. Yan, and W. Z. Li, *Solid State Ionics*, **113-115**, 291 (1998).
16. M. J. Jorgensen and M. Mogensen, *J. Electrochem. Soc.*, **148**, A433 (2001).
17. J. W. Erning, T. Hauber, U. Stimming, and K. Wippermann, *J. Power Sources*, **61**, 205 (1996).
18. Y. Takeda, R. Kanno, M. Noda, Y. Tomida, and O. Yamamoto, *J. Electrochem. Soc.*, **134**, 2656 (1987).
19. J. Vanherle, A. J. McEvoy, and K. R. Thampi, *Electrochim. Acta*, **39**, 1675 (1994).
20. A. Endo, M. Ihara, H. Komiyama, and K. Yamada, *Solid State Ionics*, **86-8**, 1191 (1996).
21. J. Winkler, P. V. Hendriksen, N. Bonanos, and M. Mogensen, *J. Electrochem. Soc.*, **145**, 1184 (1998).
22. A. C. Co, S. J. Xia, and V. I. Birss, in *Solid Oxide Fuel Cells*, S. C. Singhal and M. Dokiya, Editors, PV 2003-07, p. 478, The Electrochemical Society Proceedings Series, Pennington, NJ (2003).
23. J. O'M. Bockris and A. K. N. Reddy, *Modern Electrochemistry*, Chaps. 8 and 9, Plenum Publishing Corporation, New York (1977).
24. A. J. Bard and L. R. Faulkner, *Electrochemical Methods: Fundamentals and Applications*, Chap. 3, John Wiley & Sons, Inc., New York (2001).
25. O. Yamamoto, Y. Takeda, R. Kanno, and T. Kojima, in *Solid Oxide Fuel Cells*, S. C. Singhal, Editor, PV 89-11, p. 242, The Electrochemical Society Proceedings Series, Pennington, NJ (1989).
26. H. Yokokawa, N. Sakai, T. Kawada, and M. Dokiya, *Solid State Ionics*, **40/41**, 398 (1990).
27. R. Yue, M.Sc. Thesis, The University of Calgary, Calgary, Ontario, Canada (1997).
28. I. Epelboin, M. Ksouri, and R. Wiart, *J. Electrochem. Soc.*, **122**, 1206 (1975).
29. N. Bonanos, B. C. H. Steele, E. P. Butler, W. B. Johnson, W. L. Worrell, D. D. Mcdonald, and M. C. H. McKubre, *Impedance Spectroscopy*, p. 191, John Wiley & Sons, Inc., New York (1987).
30. A. Hammouche, Ph.D. Thesis, Institute National Polytechnique de Grenoble, France (1989).
31. A. C. Co, S. J. Xia, and V. I. Birss, in *Ionic and Mixed Conducting Ceramics*, T. A. Ramanarayanan, W. L. Worrell, and M. Mogensen, Editors, PV 2001-28, p. 141, The Electrochemical Society Proceedings Series, Pennington, NJ (2001).
32. A. C. Co, S. J. Xia, and V. I. Birss, In preparation (2004).
33. E. P. Murray, T. Tsai, and S. A. Barnett, *Solid State Ionics*, **110**, 235 (1998).
34. M. Juhl, S. Primdahl, and M. Mogensen, in *High Temperature Electrochemistry: Ceramics and Metals*, F. W. Poulsen, N. Bonanos, S. Linderoth, M. Mogensen, and B. Zachau-Christiansen, Editors, High Temperature Electrochemistry: Ceramics and Metals Conference, p. 295, Riso National Laboratory, Denmark (1996).
35. A. C. Co and V. I. Birss, In preparation (2004).
36. L. R. Velho and R. W. Bartlett, *Metall. Trans.*, **3**, 65 (1972).
37. R. Lewis and R. Gomer, *Surf. Sci.*, **12**, 157 (1968).